Computational Model for Oxygen Transport and Consumption in Human Vitreous

Benjamen A. Filas,[1] Ying-Bo Shui,[1] and David C. Beebe[1,2]

[1]Department of Ophthalmology & Visual Sciences, Washington University School of Medicine, St. Louis, Missouri
[2]Department of Cell Biology and Physiology, Washington University School of Medicine, St. Louis, Missouri

Correspondence: David C. Beebe, Department of Ophthalmology and Visual Sciences Washington University School of Medicine, Campus Box 8096, 660 S. Euclid Avenue, St. Louis, MO 63110; beebe@wustl.edu.

Submitted: June 14, 2013
Accepted: August 18, 2013

Citation: Filas BA, Shui Y-B, Beebe DC. Computational model for oxygen transport and consumption in human vitreous. *Invest Ophthalmol Vis Sci*. 2013;54:6549–6559. DOI:10.1167/iovs.13-12609

Purpose. Previous studies that measured liquefaction and oxygen content in human vitreous suggested that exposure of the lens to excess oxygen causes nuclear cataracts. Here, we developed a computational model that reproduced available experimental oxygen distributions for intact and degraded human vitreous in physiologic and environmentally perturbed conditions. After validation, the model was used to estimate how age-related changes in vitreous physiology and structure alter oxygen levels at the lens.

Methods. A finite-element model for oxygen transport and consumption in the human vitreous was created. Major inputs included ascorbate-mediated oxygen consumption in the vitreous, consumption at the posterior lens surface, and inflow from the retinal vasculature. Concentration-dependent relations were determined from experimental human data or estimated from animal studies, with the impact of all assumptions explored via parameter studies.

Results. The model reproduced experimental data in humans, including oxygen partial pressure (Po_2) gradients (≈15 mm Hg) across the anterior-posterior extent of the vitreous body, higher oxygen levels at the pars plana relative to the vitreous core, increases in Po_2 near the lens after cataract surgery, and equilibration in the vitreous chamber following vitrectomy. Loss of the antioxidative capacity of ascorbate increases oxygen levels 3-fold at the lens surface. Homogeneous vitreous degeneration (liquefaction), but not partial posterior vitreous detachment, greatly increases oxygen exposure to the lens.

Conclusions. Ascorbate content and the structure of the vitreous gel are critical determinants of lens oxygen exposure. Minimally invasive surgery and restoration of vitreous structure warrant further attention as strategies for preventing nuclear cataracts.

Keywords: vitreous, oxygen, consumption, transport, modeling, liquefaction, aging

In normal human eyes, the lens is separated from the retina by the transparent, acellular vitreous body. Functions attributed to the vitreous gel include driving growth of the eye during embryonic development and acting as a viscoelastic mechanical damper following birth.[1] Although the gel is initially homogeneous, aging leads to structural anisotropy and degeneration in the vitreous body. This process is characterized by the formation of fluid-filled spaces in the central vitreous, detachment of the vitreous from the retina, and an overall loss in water content.[2–4] Although vitreous degeneration, or liquefaction, usually occurs without incident, persistent adhesion at the vitreoretinal interface can lead to retinal tears, detachments, macular holes, and epiretinal membranes.[5]

Even when gel liquefaction and posterior vitreous detachment (PVD) occur without incident to the retina, pathophysiological changes accrue at the lens. A potential reason for this is that vitreous liquefaction (or surgical removal of the vitreous gel through pars plana vitrectomy) increases convective motion and fluid circulation in the vitreous chamber, which enhances transport of oxygen from the retina to the lens.[6] Because the retina requires a continuous supply of oxygen to support visual processes,[7] and the lens is normally in a hypoxic environment,[8] oxygen gradients exist across the vitreous body in vivo.[9–11] Following vitrectomy, oxygen content increases near the posterior lens capsule,[12] thereby increasing the risk for oxidative damage and the concurrent development of nuclear cataracts.[13] Coupled with the recently demonstrated ability of ascorbate in the vitreous gel to consume oxygen,[14] these studies collectively indicate a protective role for the intact vitreous in preventing nuclear sclerotic cataracts.

Oxygen content in the vitreous has been measured experimentally using invasive and noninvasive methods. Direct oxygen measurement in human vitreous during retinal surgery using intraocular probes requires accessing the gel through the pars plana of the ciliary body. In particular, fiber-optic sensors have provided accurate measures of oxygen content with high spatial resolution,[15] but are constrained by limitations in sampling location, due to the invasive nature of the procedure. To circumvent these issues, noninvasive magnetic resonance imaging techniques to assess vitreous oxygen content have been explored,[16] permitting the more feasible acquisition of longitudinal datasets.[17] However, limitations in precision and spatial resolution have prevented the acquisition of detailed intravitreal oxygen profiles with this method.

To address some of these experimental and technological limitations, we use a complementary, computational approach to explore oxygen distributions in the human vitreous. Similar mathematical approaches have been used to help explain

measured oxygen concentration profiles across the retina,[18–20] cornea,[21,22] and the lens capsule.[8] In particular, Linsenmeier et al.[11] studied steady-state and time-dependent oxygen distributions in feline vitreous using a 1-D Fickian diffusion analysis.[11] Building on this earlier work, here we use a finite-element approach to explore oxygen distributions in the human vitreous, including realistic eye geometry, concentration-dependent oxygen consumption in the vitreous and lens, and spatially varying retinal oxygen content, in both normal and perturbed intraocular conditions. Model inputs are chosen based on experimentally derived human data. When human data were not available, values were taken from representative animal models, with the impact of such assumptions explored via parameter studies.

We begin by determining concentration-dependent, ascorbate-mediated oxygen consumption rates in human vitreous from experimental data. Using these, and other relevant experimental data, we assemble a steady-state computational model to estimate intravitreal oxygen distributions in physiologic conditions. After showing that the model reasonably reflects experimental measurements of oxygen content, we show the impact of underlying model assumptions and parameters, and explore the effects of hyperoxic and hypoxic environmental perturbations, mimicking conditions such as long-term hyperbaric oxygen therapy and diabetic retinopathy. Lastly, we use the model to estimate how common age-related vitreous pathologies, such as liquefaction and partial vitreous detachment affect oxygen levels in the vitreous. The significance of these structural changes and their potential role in the etiology of nuclear cataracts is discussed and future opportunities for the acquisition of experimental data to improve our understanding of oxygen distribution in the vitreous are highlighted. Together, this study provides insight into how oxygen transport between the retina and lens is regulated and how common age-related changes in vitreous structure affect this process. These data should be useful for designing surgeries to resolve retinal pathology while minimizing postoperative damage to the lens.

Methods

Model Geometry and Governing Equations

An axisymmetric model for the human vitreous was created using finite-element modeling software (COMSOL Multiphysics v.4.2; The COMSOL Group, Burlington, MA) with lens geometry similar to that used in previous studies (see Fig. 2A).[23,24] The retina spans from the posterior pole to the ora serrata, located equidistant between the center of the lens and the eye equator. Finite-element meshes were made sufficiently dense such that further refinement did not significantly affect the solutions.

Steady-state oxygen transport was modeled using Fick's Law of Diffusion. In certain cases, as discussed later, we included the effects of convective motion to justify assumptions made about the absolute diffusivity of the system. Including this component gives the mass balance equation:

$$\frac{\partial c}{\partial t} + \boldsymbol{u} \cdot \nabla c = \nabla \cdot (D \nabla c) + q \qquad (1)$$

where c is oxygen concentration, $\boldsymbol{u}$ is the velocity vector, D is the diffusion coefficient for oxygen in water, and q is the ascorbate-mediated oxygen consumption of the vitreous. Because the vitreous is approximately 99% water, we take $D = 4 \times 10^{-9}$ m^2/s for oxygen in water and use Henry's Law to convert oxygen partial pressure (Po_2) to concentration, $Po_2 = k \times c$, where $k = 769.2$ L $\times$ atm/mol (584.6 m^3 $\times$ mm Hg/mol) for oxygen in water.

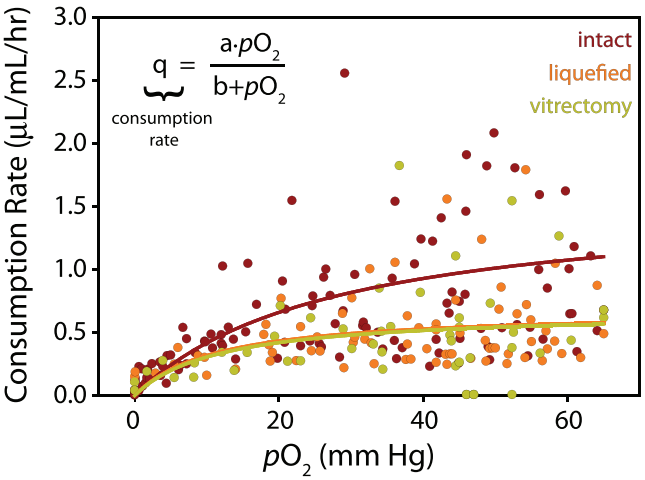

Figure 1. Ascorbate-mediated oxygen consumption in the vitreous body. Oxygen consumption rate of human vitreous ($n = 62$, up to five measurements per sample) recorded for 2 hours at 35°C in the dark. Samples were divided into three groups: intact ($n = 26$), liquefied ($n = 20$), and postvitrectomy ($n = 16$). Hyperbolic regressions provide estimates for concentration-dependent rate of ascorbate-mediated oxygen consumption in the vitreous body (intact: $a = 1.57$, $b = 27.48$; liquefied: $a = 0.68$, $b = 11.29$; vitrectomy: $a = 0.67$, $b = 11.89$).

Vitreous Structure and Ascorbate-Dependent Oxygen Consumption

In a previous study, we measured ascorbate-dependent oxygen consumption in vitreous removed at the beginning of vitrectomy surgery in a series of 62 human patients.[14] Here, we use these experimental data to estimate a concentration-dependent relationship for ascorbate-mediated oxygen consumption in the vitreous. Briefly, during a standard 3-port pars plana vitrectomy and before infusion, a 1-mL syringe was connected to the vitrectomy probe and undiluted samples (0.25–0.3 mL) were slowly drawn from the vitreous core. Samples were independently graded on a subjective 5-point elasticity scale (1 = firm gel, 5 = most fluid) by the retinal surgeon and the ocular surgeon handling the samples after removal (assessment by these two graders seldom differed). This allowed the vitreous to be divided into three groups: intact gel vitreous (gel grade ≤ 3); more liquefied vitreous (gel grade > 3); and previous vitrectomy (mixture of residual vitreous and aqueous). Following removal and grading, samples were transferred into a sealed glass tube and an optical oxygen sensor (Oxylab fiber optic oxygen sensor; Oxford Optronix Ltd., Abingdon, Oxford, UK) was inserted through a septum at one end and the rate of oxygen consumption was measured for at least 2 hours at 35°C in the dark.[14] Oxygen content in all groups (sampled at $t = 0$, 30, 60, 90, and 120 minutes) was fit with a single exponential, with the derivative of this function giving the consumption rate. Plotting rate as a function of concentration suggested that ascorbate-mediated oxygen consumption (q in Equation 1) to be reasonably approximated by a hyperbolic function (analogous to Michaelis-Menten kinetics; see Fig. 1). Because ascorbate removal by treatment of isolated vitreous with ascorbate oxidase completely eliminated the ability of the vitreous to consume oxygen, we assume that ascorbate is the sole oxygen consumer in the vitreous.[14]

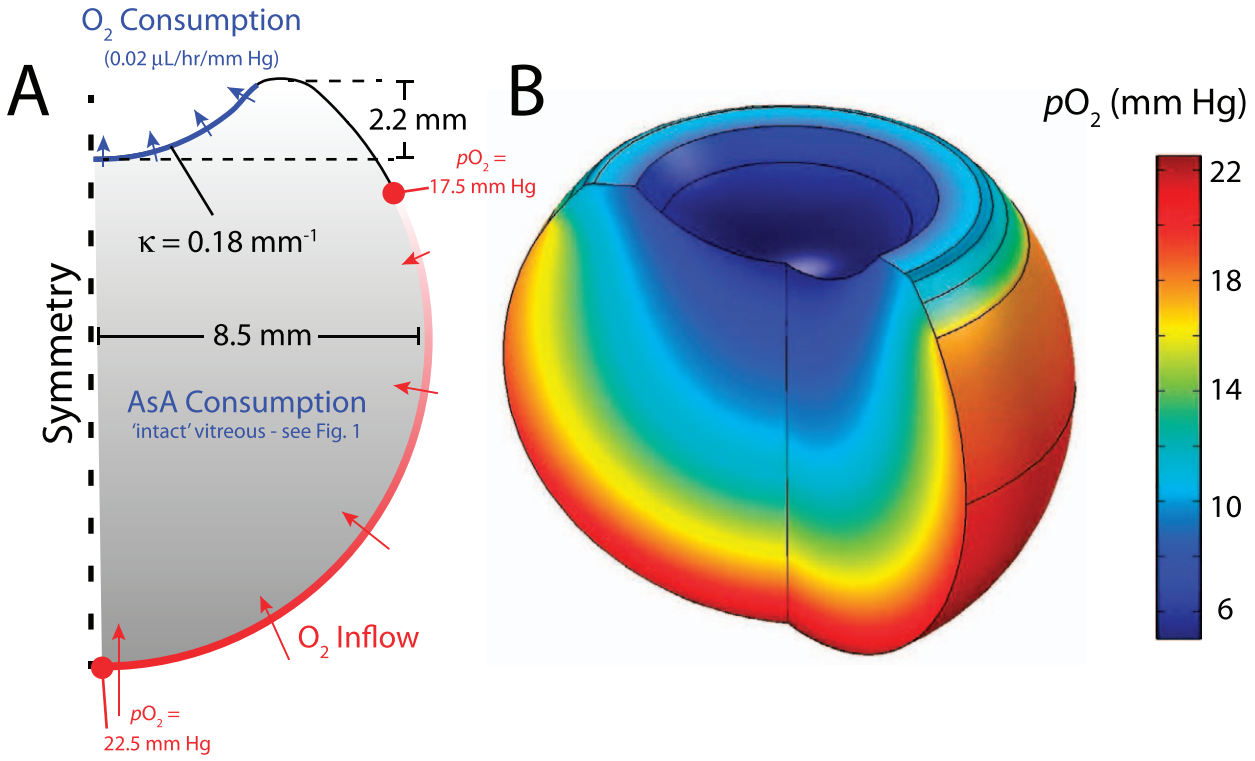

Figure 2. Modeling strategy and baseline result. **(A)** Axisymmetric, steady-state model for oxygen transport in the human vitreous. Lens indentation is anterior. Average oxygen inflow (Po_2 = 20 mm Hg) is prescribed at the retina with a mild, linearly decreasing gradient from the posterior side to the ora serrata. Concentration-dependent oxygen consumption is prescribed in the vitreous body and at the posterior surface of the lens as described in the Materials and Methods section (κ = curvature). **(B)** Baseline model result. In general, Po_2 decreases by approximately 15 mm Hg moving away from the retina and approaching the lens. Effects of individual model inputs are investigated in later simulations (Figs. 3, 4, 6).

Oxygen Consumption by the Lens

To our knowledge, oxygen consumption has not been measured in physiologic conditions in the human lens. However, a recent study in humans found increased oxygen content at locations anterior and posterior to the lens following cataract surgery compared with having an intact lens, suggesting that human lens tissue consumes oxygen.[12] In vitro studies in guinea pig and cow have also shown that the lens consumes oxygen, but consumption rates were measured in nonphysiologic (hyperoxic) conditions.[8] Alternatively, in an in vivo rabbit study, a relatively linear relationship between oxygen content and consumption rate was found across the posterior lens surface in normoxic conditions.[25] Importantly, ascorbate-mediated oxygen consumption is small in rabbits, which permits consumption rates at the posterior surface of the lens to be calculated directly without correcting for consumption in the vitreous.[14,26] As a first approximation, we use this linear relation to guide the consumption (outflow) boundary condition at the posterior side of the lens (see Fig. 2A). Because this parameter has not been measured directly in humans, we show the effects of varying the contribution of lens consumption on intravitreal oxygen content in Figure 3.

Oxygen Supply From the Inner Retina (but Not the Aqueous Humor)

The inner retina is composed of a complex network of oxygen sources (arteries, arterioles) and sinks (veins, venules) of variable length, diameter, tortuosity, and branching that vary between individuals.[27] Rather than try to model this network explicitly, we assume an average oxygen concentration at the inner retina of approximately 20 mm Hg, as previously reported.[6,7,28] (The suitability of this assumption is investigated in Fig. 5.) To our knowledge, spatial gradients in average intravitreal oxygen content ranging from the posterior pole to the ora serrata have not been quantified in humans. Previous studies found decreasing oxygen content at the vitreoretinal interface with increasing distance from the optic disk in rabbit,[25] but not in cat.[29] Magnetic resonance-based techniques in humans have remained inconclusive in this regard.[17,30,31] Therefore, we explore the effects of varying this distribution in Figure 4. For the baseline model, we assume a mild dependence of oxygen inflow with retinal position, linearly decreasing Po_2 from 22.5 mm Hg at the posterior pole to 17.5 mm Hg at the ora serrata (see Fig. 2A).

To simulate hyperoxic and hypoxic conditions, we increase or decrease the retinal oxygen profile in a stepwise manner. Previously, Holekamp et al.[10] found lower oxygen tension in the midvitreous of diabetic humans, but measurements at the vitreoretinal interface were not performed. In long-term diabetic cats, oxygen tension at the inner retina was found to be less than half that of controls.[32] On the other hand, 100% oxygen exposure increased inner retinal and vitreous Po_2 by a factor of 3 in cats (≈20–60 mm Hg), a change regulated in part by large increases in choroidal Po_2 (≈80–240 mm Hg).[33,34] As a first approximation, these experimental studies provide a Po_2 perturbation window for the hypoxia and hyperoxia simulations (up to a factor of 3).

Despite the proximity of the highly vascularized ciliary body, a recent study in humans found lower oxygen tension in the aqueous humor of the posterior chamber than in the anterior vitreous body in unoperated eyes, eyes with previous vitrectomy, and eyes with previous cataract surgery.[12] Presumably, the ciliary epithelial cells consume the majority of the oxygen delivered by the ciliary body vasculature in order to

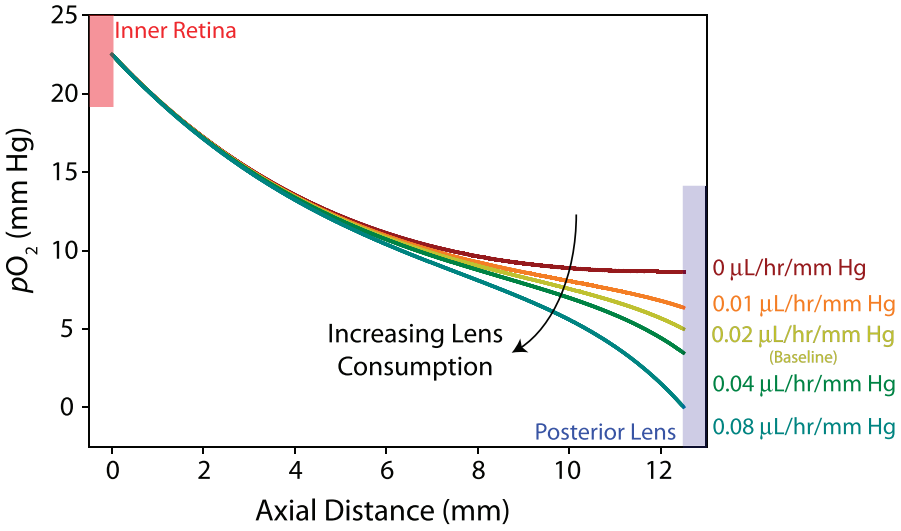

Figure 3. Lens consumption parameter study. Po_2 is plotted along the vitreous midline from the inner retina to the posterior surface of the lens. Increasing consumption decreases Po_2 in the anterior vitreous (>6 mm axial distance from the retina) with little effect on the posterior vitreous. Guided by experimental data from rabbits, we use a consumption rate of 0.02 µL/h/mm Hg as baseline (*yellow curve*) in this study.

produce the adenosine triphosphate required for aqueous secretion. The low oxygen tension in the posterior chamber would exclude the ciliary body as a source of oxygen for the anterior vitreous. Moreover, low oxygen levels were found beneath the iris, suggesting that little or no oxygen is contributed by the iris vasculature or other anterior sources (e.g., transport across the cornea) to the vitreous chamber. Hence, as a first approximation, we exclude the aqueous humor as a source of oxygen in this model.

Age-Related Changes in Oxygen Transport

Common structural changes in the vitreous that occur with age include liquefaction and detachment from the retina. Liquefaction is thought to originate in the vitreous core, as characterized by the formation of fluid-filled lacunae.[2,4,35] Several studies have shown a significant role for convective transport in Newtonian fluids occupying the vitreous chamber.[24,36,37] Because saccadic eye motions generate complex viscoelastic deformations and flow patterns that would be difficult to prescribe a priori in the model, we approximate increases in absolute oxygen diffusivity due to liquefaction (taking into account both diffusive and convective effects) by increasing the diffusion constant. To support this approach, we show that including random fluid motion (on the order of experimentally measured scleral velocities)[38] leads to comparable effects on oxygen transport (see Fig. 7). In other words, increasing the absolute diffusivity of oxygen in liquefied

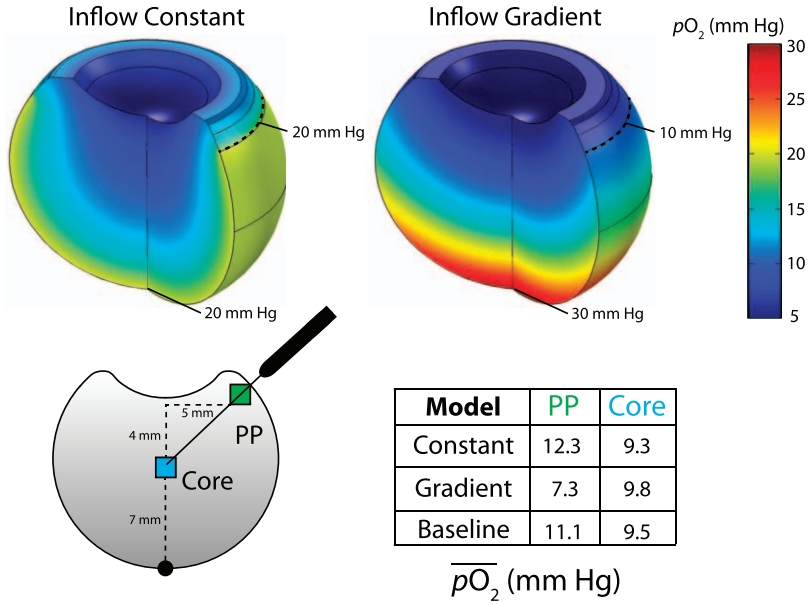

Model	PP	Core
Constant	12.3	9.3
Gradient	7.3	9.8
Baseline	11.1	9.5

Figure 4. Retinal oxygenation profile and intravitreal oxygen content. Two cases shown: (*upper left*) Po_2 = constant 20 mm Hg; (*upper right*) linear decrease in Po_2 from 30 mm Hg at the posterior pole to 10 mm Hg at the ora serrata. *Bottom*: Average oxygen content (PO_2) was recorded in a 1-mm window at the vitreous core (*blue*) and near the pars plana (PP, *green*). A strong gradient in oxygen inflow (*upper right*) leads to higher Po_2 in the core relative to the pars plana (*quantified lower right*). Constant oxygen inflow (*upper left*) or the mild gradient used in the baseline model (see Fig. 2) show the opposite trend, similar to distributions measured experimentally (*lower right*).

Investigative Ophthalmology & Visual Science

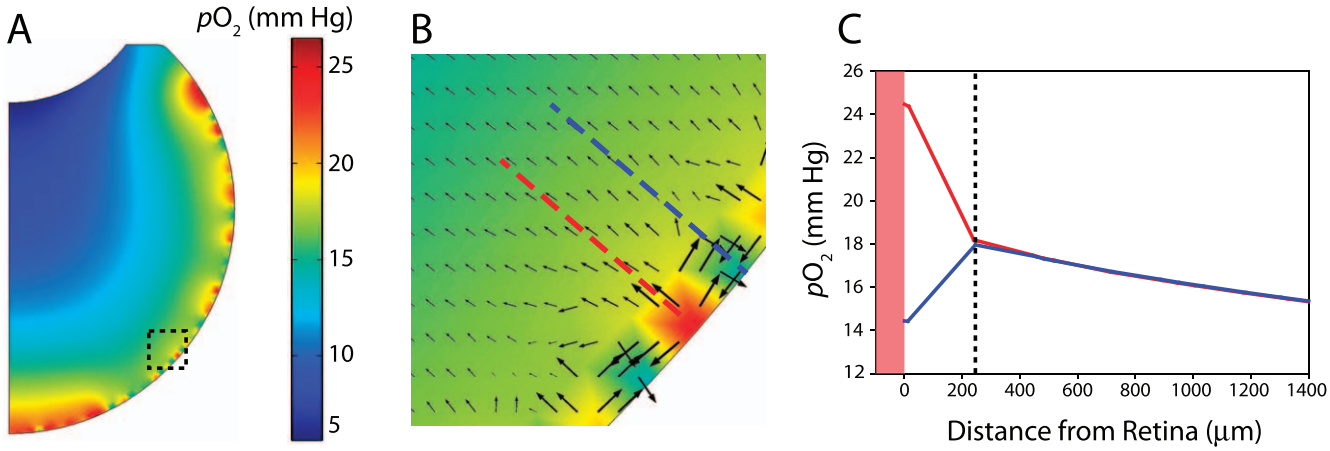

Figure 5. Investigation of homogeneous oxygen inflow assumption. (**A**) Average Po_2 of 20 mm Hg at the retina with random spatial fluctuation (±15 mm Hg; this causes the steady-state intravitreal profiles plotted here to vary by approximately ±7 mm Hg). Despite generating a physiologically unrealistic geometry, the impact of the homogeneous inflow assumption can be assessed. (**B**) Enlargement of dotted region in (**A**). *Arrow* direction and size show diffusion direction and magnitude of diffusive flux, respectively. At local sources (arteries), oxygen flows outward into the vitreous and laterally into local sinks (veins). (**C**) Intravitreal oxygen profiles normal to the retinal boundary corresponding to *dashed lines* in (**B**). In this region, local differences in oxygen content stabilize approximately 200 μm into the vitreous body.

vitreous, whether through diffusive or convective mechanisms, yields similar steady-state results. Although convective transport dominates when Newtonian fluids reside in the vitreous chamber,[36] we note that some experimental studies have reported increases in diffusive transport in liquefied relative to intact vitreous.[39]

Concurrent with liquefaction, the vitreous often detaches from the posterior retina through mechanisms that are not well understood.[40] We investigate the effect of posterior vitreous detachment on oxygen transport in the model through a change in geometry as shown in Figure 9A.

Results and Discussion

Liquefied Vitreous and Samples From Eyes With Previous Vitrectomy Consume Less Oxygen Than Intact Vitreous

In a previous study, we measured the rate of ascorbate-mediated oxygen consumption in human vitreous during 2 hours of incubation immediately following vitrectomy. To simplify the analysis in that study, consumption rates were only reported during the first half hour of testing and concentration-dependent effects were not considered in the analysis. Here, we reanalyze these data, fitting the raw oxygen consumption data with single exponential curves ($n = 62$ samples). The closed form derivatives of these curves give the oxygen consumption rates for each sample at the experimentally measured oxygen concentrations. The results of this analysis are shown in Figure 1. Samples are divided into three groups as previously described: samples from intact vitreous ($n = 26$), more liquefied vitreous ($n = 20$), and those from eyes with previous vitrectomy ($n = 16$). Rapid increases in consumption rate between 0 and 10 mm Hg of oxygen followed by rate stabilization at higher oxygen concentrations was indicative of Michaelis-Menten like reaction kinetics, as previously proposed.[41–43] Hence, consumption data were fit with a single hyperbolic function (see Fig. 1) to mathematically estimate concentration-dependent ascorbate-mediated oxygen consumption rates between groups. Consistent with our earlier analysis, we found ascorbate-mediated oxygen consumption to be highest in intact vitreous with similar consumption rates found in liquefied vitreous and samples from eyes with previous vitrectomy (Fig. 1).[14] Previously, we hypothesized that constant transport of ascorbate into the vitreous, combined with increased oxygen transport and mixing due to vitreous liquefaction, results in the lower ascorbate levels and the slower oxygen consumption rates observed in liquefied samples.[14]

Computational Model Predicts Intravitreal Oxygen Content Similar to Experimental Measurements

As outlined in the Materials and Methods section, we developed an axisymmetric, steady-state, finite-element model for oxygen transport and consumption in the human vitreous (Fig. 2A). In the baseline model, intravitreal oxygen content is determined by three parameters: oxygen inflow at the inner retinal boundary, ascorbate-mediated oxygen consumption in the vitreous body, and oxygen consumption (outflow) at the posterior of the lens. An average Po_2 of 20 mm Hg is assumed at the retinal surface with a mild concentration gradient from the posterior pole approaching the ora serrata. Ascorbate-mediated oxygen consumption in the vitreous body is prescribed using the hyperbolic relation determined for intact vitreous (Fig. 1). At the posterior lens surface, a linear oxygen consumption rate with concentration (0.02 μL/h/mm Hg of oxygen) is specified as found previously in rabbits.[25] Using these parameters, the model yields steady-state oxygen distributions in good agreement to those measured experimentally (Fig. 2B). Oxygen tension rapidly decreases moving away from the retinal surface into the vitreous,[44,45] with Po_2 decreasing over 15 mm Hg from the retina approaching the posterior surface of the lens.[6] Average oxygen content at the pars plana is greater than the vitreous core,[10] with similar concentrations to those measured experimentally (≈10 mm Hg).[9]

While ascorbate-mediated oxygen consumption in the vitreous body was calculated directly from experimental measurements in humans, consumption at the posterior surface of the lens was estimated from in vivo rabbit data.[25] In the model, varying the concentration-dependent oxygen consumption rate at the posterior lens surface only affected oxygen content in the anterior half of the vitreous, with oxygen content near the lens reaching negligible quantities at a

Investigative Ophthalmology & Visual Science

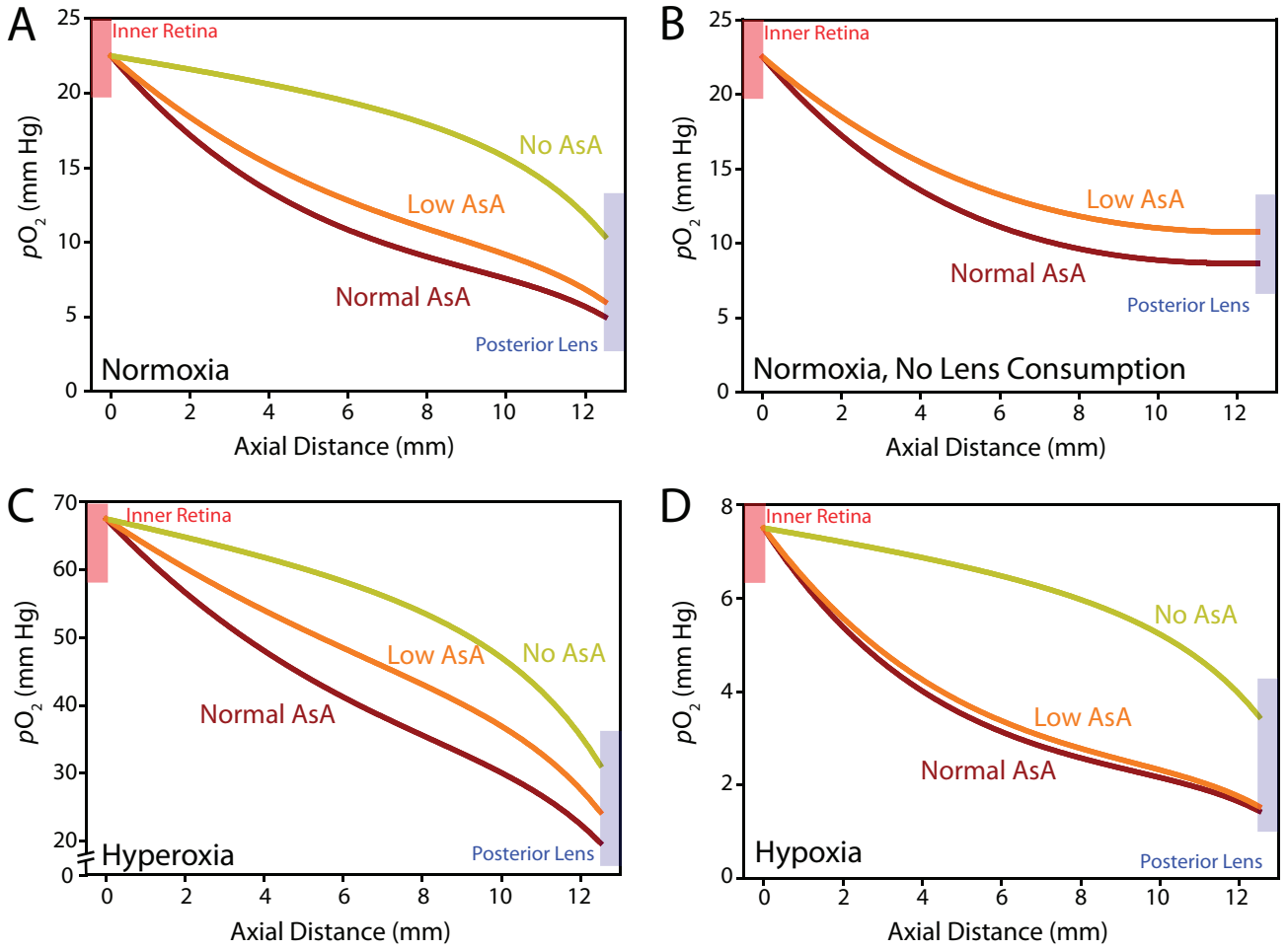

Figure 6. Ascorbate-mediated oxygen consumption. (**A**) Effect of AsA on intravitreal oxygen content including effects due to lens consumption. Normal and low AsA, refer to consumption rates in intact and liquefied vitreous, respectively, as estimated from experimental data (see Fig. 1). (**B**) Same analysis with no lens consumption. (In this case, with no AsA consumption intravitreal oxygen content would be determined only by prescribed inflow.) (**C**) Ascorbate-mediated oxygen consumption in hyperoxic (inflow tripled) conditions. (**D**) In hypoxic conditions, one third of the original oxygen inflow prescribed.

consumption rate of 0.08 μL/h/mm Hg (four times baseline; Fig. 3). Qualitatively, curve shape switched from exponentially decreasing to sigmoidal as lens consumption rates increased. Oxygen content at the posterior surface of the lens was approximately 3 mm Hg lower in the baseline model (0.02 μL/h/mm Hg) relative to the no consumption case, similar to differences in oxygen content measured in phakic and pseudophakic patients.[12] This result suggested that the lens consumption rate estimated from rabbit data was a reasonable approximation for the human lens.

Next, we explored the impact of the spatial distribution of average oxygen inflow at the inner retina. Recall that in the baseline model we assume a mild Po_2 gradient from 22.5 mm Hg at the posterior pole to 17.5 mm Hg at the ora serrata. Here, we compare two additional distributions: constant Po_2 of 20 mm Hg at the retinal boundary, similar to cats,[29] and maximum Po_2 of 30 mm Hg at the posterior pole with a linear decrease to 10 mm Hg at the ora serrata, similar to gradients found in rabbits (Fig. 4).[25] Oxygen profiles were qualitatively different, with a U-shaped profile in the constant inflow case (Fig. 4, upper left) and a smoother distribution in the graded model (Fig. 4, upper right). Constant oxygen inflow at the retinal surface led to a decrease in Po_2 of approximately 3 mm Hg ranging from the edge to the center of the lens (Fig. 4, upper left). In the high retinal inflow gradient model, however, Po_2 was more homogeneous across the lens surface (≈1 mm Hg spatial variation; Fig. 4, upper right).

In two previous experimental studies, Holekamp et al.[9,10] measured average oxygen content in the vitreous core and near the probe insertion point at the pars plana (Fig. 4, lower left). These studies found a highly significant difference between regions ($P < 0.003$), with oxygen content approximately 2 mm Hg greater near the pars plana relative to the vitreous core. We computationally repeated this measurement by averaging oxygen content in a 1-mm window inside these regions (Fig. 4, lower right). Oxygen content was lower in the vitreous core relative to the pars plana in both the constant inflow and baseline models (owing to the U-shaped distributions), with the opposite result found in the high inflow gradient model. Together, these results suggest either a constant oxygen inflow or a mild gradient to be reasonable first approximations for average oxygen content at the retinal surface.

To help validate our underlying assumption that local differences in oxygen content due to the presence of arteries, arterioles, veins, and venules could be neglected outside regions immediately adjacent to the retina, we prescribed an average Po_2 of 20 mm Hg at the retinal boundary, but with random spatial fluctuations (±15 mm Hg) to generate sources and sinks (Fig. 5A). Although this generates physiologically unrealistic vessel distributions due to the axisymmetric

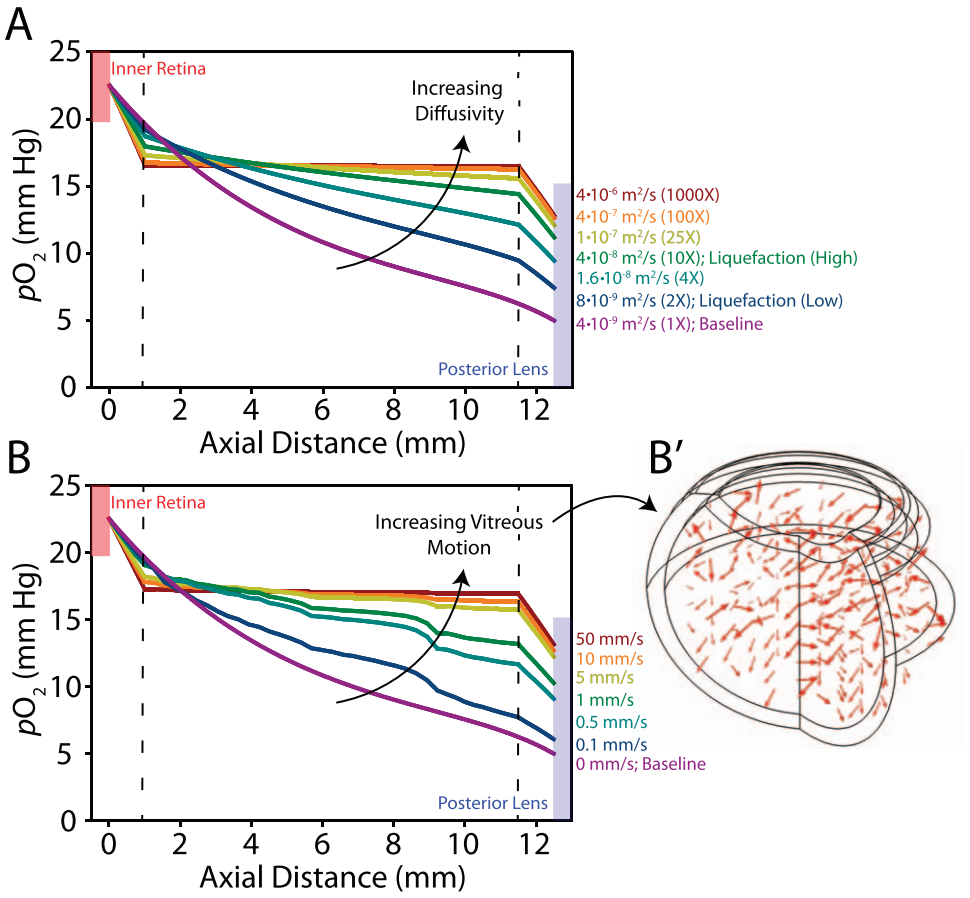

Figure 7. Diffusivity and fluid mixing in the vitreous body. One millimeter of peripheral vitreous is intact with increased diffusivity or random motion prescribed in the core. **(A)** With increasing diffusivity, oxygen content is nearly homogeneous in the core with steep concentration gradients present near the retina and lens. Diffusion constants for each simulation indicated on the right. Two-fold and 10-fold increases in the diffusion constant are used in later simulations of "low" and "high" liquefaction, respectively. **(B)** Similar trends are observed with random motion prescribed in the core. Maximum velocities for each simulation indicated on the right. **(B′)** *Arrows* indicate direction and relative magnitude of prescribed motion.

geometry, the impact of locally inhomogeneous versus spatially averaged oxygen inflow could be estimated with this approach. Similar to the baseline model, we found average Po_2 to drop to near 5 mm Hg at the posterior surface of the lens, as well as the characteristic U-shaped oxygen distribution outside the retinal vicinity (Fig. 5A). When prospective arteries were surrounded by veins, oxygen was transported outward from the artery into the vitreous and laterally into the veins (Fig. 5B), as previously proposed,[6] with intravitreal content normalizing within 200 to 500 μm of the retinal surface (Fig. 5C), as observed experimentally.[44,45] Results from this simulation supported our assumption that average oxygen inflow is a reasonable simplification when investigating intravitreal oxygen content outside of the immediate vicinity of the inner retinal surface. Moreover, several salient local transport effects were captured in the model, providing additional support for the suitability of the finite-element approach taken in this study.

In summary, we developed a finite-element model for oxygen transport in the human vitreous that predicts oxygen distributions similar to those measured experimentally. Ascorbate-mediated oxygen consumption in the vitreous body is determined directly from experimental data, while consumption at the lens surface and retinal inflow are estimated from animal studies. Such parameters are shown to be reasonable first approximations through comparison with relevant human data. Next, we use the model as a tool to explore how ascorbic acid-mediated oxygen consumption and age-related changes in vitreous structure affect oxygen levels at the posterior surface of the lens.

Ascorbic Acid Is an Important Regulator of Intravitreal Oxygen Content

Using the baseline model (Fig. 2), we explored the effect of ascorbic acid (AsA)-mediated oxygen consumption in normal and perturbed environmental conditions. In normoxic conditions, AsA content was critical to reducing oxygen levels at the lens, as oxygen content tripled at the posterior of the lens when no ascorbate-mediated antioxidative capacity was prescribed in the vitreous (Fig. 6A). Differences were comparatively lower between the normal and lower AsA conditions (see Fig. 1), suggesting that the antioxidative capacity of the degraded vitreous may still provide a significant source of oxygen consuming activity in physiologic conditions (Fig. 6A). If the oxygen-consuming ability of the lens is reduced (e.g., due to possible age-related changes; Fig. 6B) or the eye is exposed to prolonged hyperoxia (Fig. 6C), differences in antioxidative capacity between intact and degraded vitreous are more substantial. On the other hand, in the case of reduced oxygen inflow (e.g., diabetic retinopathy), differences between high and low AsA on intravitreal oxygen content were negligible, but AsA-mediated consumption still played an

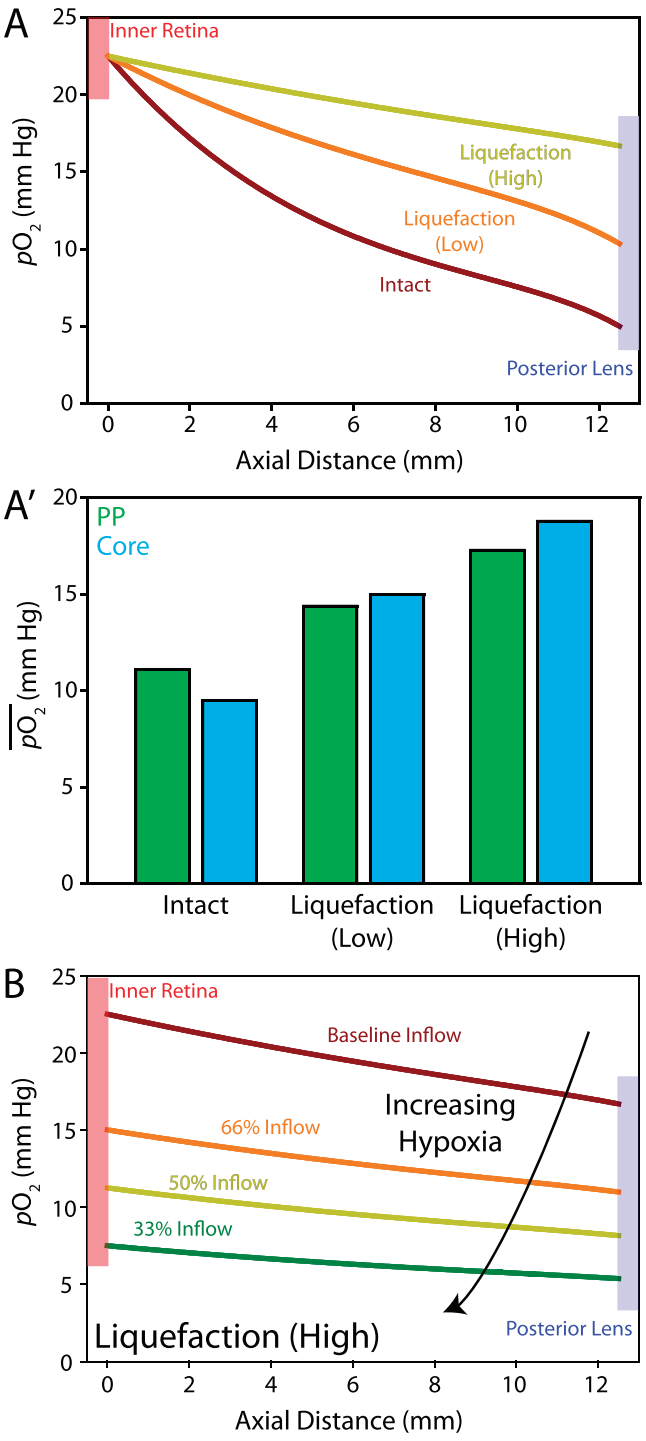

Figure 8. Vitreous liquefaction in normoxic and hypoxic conditions. (**A**) Normoxia: Vitreous liquefaction increases Po_2 at the lens by a factor of 2 to 4 depending on severity. (**A′**) With increasing liquefaction, average Po_2 at the vitreous core (*blue*) begins to exceed the PP (*green*) region. (**B**) In the case of high vitreous liquefaction, retinal hypoxia substantially decreases the amount of oxygen reaching lens, even in only moderately hypoxic conditions.

important role in consuming oxygen (Fig. 6D). Together, these simulations suggest that AsA-mediated oxygen consumption is critical to limit oxidative damage to the lens. Differences in AsA content between intact and liquefied vitreous change intravitreal oxygen profiles, with differences becoming most significant when oxygen content in the vitreous is increased (e.g., through reduced lens consumption or hyperoxic conditions).

Liquefaction, but Not Posterior Partial Vitreous Detachment, as a Major Risk Factor for Oxidative Damage to the Lens

Lastly, we estimated the impact of common age-related structural changes in the vitreous body (liquefaction and partial posterior vitreous detachment [PVD]) on intravitreal oxygen content. As described in the Methods section, our goal was to simulate liquefaction through increasing the absolute diffusivity of the vitreous body (including transport effects due to both diffusion and convection). As a test case, we developed a model with 1 mm of intact vitreous surrounding a degraded (liquid) core (Fig. 7). Increasing the diffusion coefficient from baseline (Fig. 7A, purple curve) caused oxygen content in the core to equilibrate, with solutions converging at a diffusion coefficient three orders of magnitude greater than baseline (Fig. 7A, red curve). Prescribing random motion in the vitreous core showed a similar trend with solutions converging at flow velocities approaching 5 mm/s (Fig. 7B, 7B′). Importantly, this convergence behavior was mesh-independent and consistent when alternative random flow patterns were prescribed. Because both perturbations produced similar qualitative trends, for better reproducibility and convergence we prescribed vitreous liquefaction by increasing the diffusion constant (D in Equation 1) in subsequent simulations. For comparison, we used two cases: low (D doubled; Fig. 7A, blue curve) and high (D increased by one order of magnitude; Fig. 7A, green curve) liquefaction. These values were chosen to illustrate the effects of a relatively small increase in the absolute diffusivity of the system and a substantial increase, near the point where oxygen distributions converge and additional "liquefaction" has negligible effects (Fig. 7). In subsequent simulations for both cases, low AsA content was prescribed in tandem with liquefaction, as observed experimentally (see Fig. 1; liquefied condition).

Regardless of the severity of liquefaction, degeneration greatly increased oxygen content in the vitreous (Fig. 8A), approximately doubling and quadrupling oxygen levels near the lens in cases of low and high liquefaction, respectively. This result is supported by experimental studies that have shown a strong correlation between vitreous degeneration and lens nuclear opacification.[13] In addition to increasing overall content, liquefaction also changed the distribution of oxygen in the vitreous. Using the approach described in Figure 4, we found that with increasing liquefaction, oxygen tension increased in the vitreous core relative to the pars plana (along with overall magnitude) due to equilibration, similar to trends observed experimentally following vitrectomy surgery (Fig. 8A′).[9] As another test, we repeated the high liquefaction simulation in increasingly hypoxic conditions (Fig. 8B). With inflow conditions set at one-third of baseline (Fig. 8B, green curve), Po_2 at the lens was nearly identical to intact, normal vitreous, while inflow two-thirds of baseline decreased oxygen exposure more than 5 mm Hg at the lens (Fig. 8B, red curve). These simulations suggested that in the case of significant liquefaction, even small decreases in retinal oxygenation can protect the lens from oxidative damage. This result is supported by a recent study reporting no significant progression in nuclear opacity 1 year postvitrectomy in patients with ischemic diabetic retinopathy.[46]

Another common age-related change to the vitreous body is PVD from the retina. Here, we specified a large posterior PVD (Fig. 9A) with high liquefaction in the detached region. The remaining vitreous is specified to be intact (Fig. 9B) or mildly

Investigative Ophthalmology & Visual Science

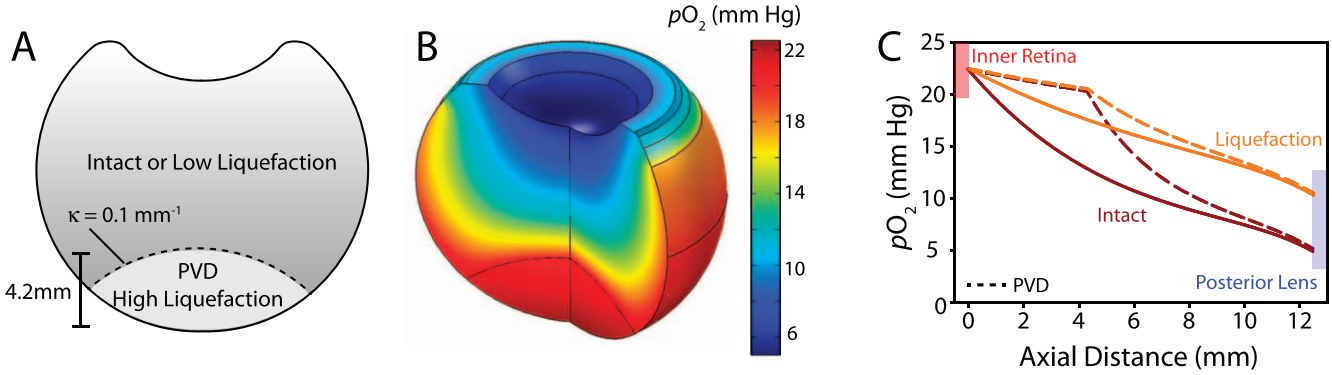

Figure 9. Partial PVD. (**A**) Geometry for PVD used in the simulation. In the detached region, high liquefaction is assumed with either an intact or slightly liquefied vitreous body (κ = curvature). (**B**) Model result assuming intact vitreous body. (**C**) In PVD simulations (*dashed lines*), oxygen content is high and relatively homogeneous in the detached region (up to 4.2 mm from the inner retina). Regardless of whether the remaining vitreous is assumed to be intact (*red*) or mildly liquefied (*orange*), PVD has little effect on oxygen levels at the lens.

degraded (low liquefaction condition, see Figs. 7, 8), as PVD often occurs concurrently with vitreous degeneration. The model predicts posterior PVD to have a negligible effect on oxygen content at the lens in both intact and liquefied vitreous (Fig. 9C). These results suggest structural degeneration of the vitreous body, but not the presence of a posterior PVD alone, as a significant risk factor for exposure of the lens to excess oxygen.

Conclusions and Limitations

Liquefaction and surgical removal of the vitreous via pars plana vitrectomy are known risk factors for the development of nuclear cataracts, a disease caused in part by oxidative damage to the lens. Although oxygen distributions in intact and liquefied human vitreous in physiologic and hypoxic conditions have been explored experimentally, these data have not been assimilated into a computational model to unify these analyses. Here, we integrated measures of retinal inflow, lens consumption, and ascorbate-mediated vitreous consumption into a steady-state model for oxygen transport that reasonably reproduces experimental oxygen distributions in normal and liquefied vitreous, as well as in perturbed environmental conditions (Figs. 2–4, 8). This approach provides mathematical backing and synthesis to previous investigations, allowing individual system components to be analyzed in a controlled fashion, tests often difficult to perform experimentally. Moreover, predictive insight into the etiology of nuclear cataracts is gained from the model, as illustrated by the impacts of ascorbate-mediated consumption, vitreous liquefaction, and partial vitreous detachment on oxygenation levels at the lens (Figs. 6, 8, 9).

In developing the baseline model, experimental data from aged humans were used, and as such, results presented here are most relevant in comparing oxygen content between intact and degenerated adult vitreous. Indeed, it is likely that lens and vitreous consumption rates may be higher in children, where age-related structural and physiological changes have not accrued.[14] Compensatory mechanisms may be present in younger patients, perhaps explaining why this population is better protected from nuclear cataracts postvitrectomy or after hyperbaric oxygen treatment.[9] To our knowledge, however, vitreous oxygen distributions have not been measured in children and young adults, precluding the effects of early aging from being fully assessed. Metabolic changes in lens consumption and retinal inflow that occur with age are similarly not well understood and not included in the simulations. Despite these limitations, the effects of age-related changes on these processes (e.g., decreases in lens consumption [Fig. 3] and retinal inflow [Figs. 6D, 8A′] can be estimated here, providing a starting point for future experimental and computational efforts.

Not directly addressed in the current study are the dynamics of oxygen transport across the posterior chamber. We found low oxygen tension (≈8 mm Hg) in the most anterior vitreous near its interface with the posterior chamber (Fig. 2B), in reasonable agreement with a past study that measured Po_2 well inside the posterior chamber to be near 5 mm Hg.[12] These relatively small differences in oxygen content support a "no flux" boundary condition between the vitreous and posterior chambers as a reasonable first approximation. Future experimental and computational efforts should more accurately characterize the dynamics of oxygen transport across this boundary and inside the posterior chamber, including oxygen inflow from the ciliary body and iris vasculatures, lens consumption, ascorbate content in the aqueous, as well as transport between the posterior and anterior chambers.

Here, and in a related study,[14] we showed that liquefied vitreous maintains antioxidative abilities (Figs. 1, 6A), despite lower levels of ascorbate in degraded (≈1.2 mM), relative to intact vitreous (≈2.0 mM). Because liquefied vitreous retains this antioxidative ability, we speculate that most of the oxidative damage that occurs to the lens with age may be due to enhanced convective transport (Fig. 8). Using realistic viscoelastic material properties, future studies should more accurately assess the effects of fluid mixing on oxygen transport during eye movements in intact and degraded (e.g., aged or pharmacologically digested) vitreous. Although it was beyond the scope of the present study to explicitly model the effects of intravitreal flow following liquefaction, with our current approach, we delineated an appropriate liquefaction range and showed that even modest degeneration can substantially increase oxygen content at the lens.

Results from this study also highlight important future directions for cataract prevention, namely preserving, or restoring the structure of the vitreous body. Because posterior PVD did not significantly affect oxygen levels at the lens in intact and slightly liquefied vitreous (Fig. 9), it can be inferred that procedures aimed at preserving the anterior half of the vitreous body may be rational approaches for mitigating or delaying the onset of nuclear cataracts. This analysis would predict that limited, or minimally destructive, vitreous surgeries (as opposed to full vitrectomy) could greatly maintain postoperative lens function. Moreover, if pharmacologic vitreolysis is used,[47] future work should focus on targeting

these digestions locally to problematic regions (e.g., sites of vitreoretinal traction) as opposed to digesting the entire vitreous. Lastly, these results predict that delaying or reversing biomechanical changes that occur to the vitreous with age to be an important pharmacologic target for improving long-term ocular health.

In summary, we have developed a steady-state, finite-element model for oxygen transport in the vitreous. The model captures intravitreal oxygen content similar to experiments in normal conditions, as well as following biophysical and environmental perturbations. These results demonstrate the importance of ascorbic acid as a vitreous antioxidant and support liquefaction and associated enhanced convective transport between the retina and lens as a major mechanism for nuclear cataract postvitrectomy. Future work should focus on developing minimally invasive vitreous surgery techniques and restorative treatments for degraded vitreous.

Acknowledgments

We thank Robert Linsenmeier (Northwestern University) and Matthew Wyczalkowski (Washington University) for their helpful discussions.

Supported by the National Eye Institute Grants EY013360 (BAF), EY021515 (Y-BS), and Core Grant EY02687, and by an unrestricted grant from Research to Prevent Blindness to the Department of Ophthalmology and Visual Science.

Disclosure: **B.A. Filas**, None; **Y.-B. Shui**, None; **D.C. Beebe**, None

References

1. Nickerson CS, Park J, Kornfield JA, Karageozian H. Rheological properties of the vitreous and the role of hyaluronic acid. *J Biomech*. 2008;41:1840–1846.
2. Sebag J. Age-related changes in human vitreous structure. *Graefe's Arch Clin Exp Ophthalmol*. 1987;225:89–93.
3. Los LI, Van der Worp RJ, Van Luyn MJA, Hooymans JMM. Age-related liquefaction of the human vitreous body: LM and TEM evaluation of the role of proteoglycans and collagen. *Invest Ophthalmol Vis Sci*. 2003;44:2828–2833.
4. Le Goff MM, Bishop PN. Adult vitreous structure and postnatal changes. *Eye*. 2008;22:1214–1222.
5. Sebag J. Age-related differences in the human vitreoretinal interface. *Arch Ophthalmol*. 1991;109:966–971.
6. Beebe DC, Holekamp NM, Siegfried C, Shui Y-B. Vitreoretinal influences on lens function and cataract. *Philos Transact B Biol Sci*. 2011;366:1293–1300.
7. Wangsa-Wirawan ND, Linsenmeier RA. Retinal oxygen: fundamental and clinical aspects. *Arch Ophthalmol*. 2003;121:547–557.
8. McNulty R, Wang H, Mathias RT, Ortwerth BJ, Truscott RJW, Bassnett S. Regulation of tissue oxygen levels in the mammalian lens. *J Physiol*. 2004;559(pt 3):883–898.
9. Holekamp NM, Shui Y-B, Beebe DC. Vitrectomy surgery increases oxygen exposure to the lens: a possible mechanism for nuclear cataract formation. *Am J Ophthalmol*. 2005;139:302–310.
10. Holekamp NM, Shui Y-B, Beebe D. Lower intraocular oxygen tension in diabetic patients: possible contribution to decreased incidence of nuclear sclerotic cataract. *Am J Ophthalmol*. 2006;141:1027–1032.
11. Linsenmeier RA, Goldstick TK, Blum RS, Enroth-Cugell C. Estimation of retinal oxygen transients from measurements made in the vitreous humor. *Exp Eye Res*. 1981;32:369–379.
12. Siegfried CJ, Shui Y-B, Holekamp NM, Bai F, Beebe DC. Oxygen distribution in the human eye: relevance to the etiology of open-angle glaucoma after vitrectomy. *Invest Ophthalmol Vis Sci*. 2010;51:5731–5738.
13. Harocopos GJ, Shui Y-B, McKinnon M, Holekamp NM, Gordon MO, Beebe DC. Importance of vitreous liquefaction in age-related cataract. *Invest Ophthalmol Vis Sci*. 2004;45:77–85.
14. Shui Y-B, Holekamp NM, Kramer BC, et al. The gel state of the vitreous and ascorbate-dependent oxygen consumption: relationship to the etiology of nuclear cataracts. *Arch Ophthalmol*. 2009;127:475–482.
15. Park Y-H, Shui Y-B, Beebe DC. Comparison of two probe designs for determining intraocular oxygen distribution. *Br J Ophthalmol*. 2011;95:118–122.
16. Berkowitz BA, McDonald C, Ito Y, Tofts PS, Latif Z, Gross J. Measuring the human retinal oxygenation response to a hyperoxic challenge using MRI: eliminating blinking artifacts and demonstrating proof of concept. *Magn Reson Med*. 2001;46:412–416.
17. Simpson ARH, Dowell NG, Jackson TL, Tofts PS, Hughes EH. Measuring the effect of pars plana vitrectomy on vitreous oxygenation using magnetic resonance imaging. *Invest Ophthalmol Vis Sci*. 2013;54:2028–2034.
18. Dollery CT, Bulpitt CJ, Kohner EM. Oxygen supply to the retina from the retinal and choroidal circulations at normal and increased arterial oxygen tensions. *Invest Ophthalmol Vis Sci*. 1969;8:588–594.
19. Braun RD, Linsenmeier RA, Goldstick TK. Oxygen consumption in the inner and outer retina of the cat. *Invest Ophthalmol Vis Sci*. 1995;36:542–554.
20. Cringle S, Yu DY, Alder V, Su EN, Yu P. Oxygen consumption in the avascular guinea pig retina. *Am J Ophthalmol*. 1996;271(3 pt 2):H1162–H1165.
21. Fatt I, Bieber MT. The steady-state distribution of oxygen and carbon dioxide in the in vivo cornea. I. The open eye in air and the closed eye. *Exp Eye Res*. 1968;7:103–112.
22. Larrea X, Büchler P. A transient diffusion model of the cornea for the assessment of oxygen diffusivity and consumption. *Invest Ophthalmol Vis Sci*. 2009;50:1076–1080.
23. Stay MS, Xu J, Randolph TW, Barocas VH. Computer simulation of convective and diffusive transport of controlled-release drugs in the vitreous humor. *Pharm Res*. 2003;20:96–102.
24. Balachandran RK, Barocas VH. Contribution of saccadic motion to intravitreal drug transport: theoretical analysis. *Pharm Res*. 2011;28:1049–1064.
25. Shui Y-B, Fu J-J, Garcia C, et al. Oxygen distribution in the rabbit eye and oxygen consumption by the lens. *Invest Ophthalmol Vis Sci*. 2006;47:1571–1580.
26. Zhang XM, Ohishi K, Hiramitsu T. Microdialysis measurement of ascorbic acid in rabbit vitreous after photodynamic reaction. *Exp Eye Res*. 2001;73:303–309.
27. Martinez-Perez ME, Hughes AD, Stanton AV, et al. Retinal vascular tree morphology: a semi-automatic quantification. *IEEE Trans Biomed Eng*. 2002;49:912–917.
28. Sakaue H, Negi A, Honda Y. Comparative study of vitreous oxygen tension in human and rabbit eyes. *Invest Ophthalmol Vis Sci*. 1989;30:1933–1937.
29. Uyama C. Diffusion model of a cat eye. In: Kessler M, ed. *Oxygen Supply: Theoretical and Practical Aspects of Oxygen Supply and Microcirculation of Tissue*. Munich, Germany: Urban & Schwarzenberg; 1973:64–66.
30. Trick GL, Edwards P, Desai U, Berkowitz BA. Early supernormal retinal oxygenation response in patients with diabetes. *Invest Ophthalmol Vis Sci*. 2006;47 :1612–1619.
31. Zhang Y, Peng Q, Kiel JW, Rosende CA, Duong TQ. Magnetic resonance imaging of vascular oxygenation changes during hyperoxia and carbogen challenges in the human retina. *Invest Ophthalmol Vis Sci*. 2011;52:286–291.

Investigative Ophthalmology & Visual Science

32. Linsenmeier RA, Braun RD, McRipley MA, et al. Retinal hypoxia in long-term diabetic cats. *Invest Ophthalmol Vis Sci*. 1998;39:1647–1657.
33. Linsenmeier RA, Yancey CM. Effects of hyperoxia on the oxygen distribution in the intact cat retina. *Invest Ophthalmol Vis Sci*. 1989;30:612–618.
34. Linsenmeier R. Oxygen measurements in animals. In: Schmetterer L, Kiel JW, eds. *Ocular Blood Flow*. New York, NY: Springer-Verlag Berlin Heidelberg; 2012:65–93.
35. Sebag J, Balazs EA. Morphology and ultrastructure of human vitreous fibers. *Invest Ophthalmol Vis Sci*. 1989;30:1867–1871.
36. Stocchino A, Repetto R, Siggers JH. Mixing processes in the vitreous chamber induced by eye rotations. *Phys Med Biol*. 2010;55:453–467.
37. Repetto R, Siggers JH, Stocchino A. Mathematical model of flow in the vitreous humor induced by saccadic eye rotations: effect of geometry. *Biomech Model Mechanobiol*. 2010;9:65–76.
38. Rossi T, Querzoli G, Pasqualitto G, et al. Ultrasound imaging velocimetry of the human vitreous. *Exp Eye Res*. 2012;99:98–104.
39. Gisladottir S, Loftsson T, Stefansson E. Diffusion characteristics of vitreous humour and saline solution follow the Stokes Einstein equation. *Graefes Arch Clin Exp Ophthalmol*. 2009;247:1677–1684.
40. Bishop PN. Structural macromolecules and supramolecular organisation of the vitreous gel. *Prog Retin Eye Res*. 2000;19:323–344.
41. Sengers BG, Van Donkelaar CC, Oomens CWJ, Baaijens FPT. Computational study of culture conditions and nutrient supply in cartilage tissue engineering. *Biotechnol Prog*. 2005;21:1252–1261.
42. Van Vlimmeren MAA, Driessen-Mol A, Oomens CWJ, et al. Low oxygen concentrations impair tissue development in tissue-engineered cardiovascular constructs. *Tissue Eng Part A*. 2012;18:221–231.
43. Buchwald P. FEM-based oxygen consumption and cell viability models for avascular pancreatic islets. *Theor Biol Med Model*. 2009;6:5.
44. Alder VA, Cringle SJ. The effect of the retinal circulation on vitreal oxygen tension. *Curr Eye Res*. 1985;4:121–129.
45. Alder VA, Niemeyer G, Cringle SJ, Brown MJ. Vitreal oxygen tension gradients in the isolated perfused cat eye. *Curr Eye Res*. 1986;5:249–256.
46. Holekamp NM, Bai F, Shui Y-B, Almony A, Beebe DC. Ischemic diabetic retinopathy may protect against nuclear sclerotic cataract. *Am J Ophthalmol*. 2010;150:543–550.e1.
47. Stalmans P, Benz MS, Gandorfer A, et al. Enzymatic vitreolysis with ocriplasmin for vitreomacular traction and macular holes. *N Engl J Med*. 2012;367:606–615.

Investigative Ophthalmology & Visual Science